Experimental Demonstration of 84 Gb/s PAM-4 Over up to 1.6 km SSMF Using a 20-GHz VCSEL at 1525 nm

Eiselt, Nicklas; Griesser, Helmut; Wei, Jinlong; Hohenleitner, Robert; Dochhan, Annika ; Ortsiefer, Markus; Eiselt, Michael H.; Neumeyr, Christian; Vegas Olmos, Juan José; Tafur Monroy, Idelfonso

Published in:
Journal of Lightwave Technology

Link to article, DOI:
10.1109/JLT.2017.2662800

Publication date:
2017

Document Version
Peer reviewed version

Experimental Demonstration of 84 Gb/s PAM-4 over up to 1.6 km SSMF Using a 20-GHz VCSEL at 1525 nm

Nicklas Eiselt, Helmut Griesser, Jinlong Wei, Robert Hohenleitner, Annika Dochhan, Markus Ortsiefer, Michael H. Eiselt, Christian Neumeyr, Juan José Vegas Olmos, and Idelfonso Tafur Monroy

***Abstract* – We demonstrate 84 Gb/s four-level pulse amplitude modulation (PAM-4) over up to 1.6 km standard single mode fiber (SSMF) using a 20-GHz single mode short cavity vertical cavity surface emitting laser diode (VCSEL) at a transmission wavelength of 1525 nm. Different equalizer approaches including a common feedforward equalizer (FFE), a non-linear Volterra equalizer (NLVE), a maximum likelihood sequence estimator (MLSE) and their combinations are evaluated working either as an equalizer for a standard PAM-4 or a partial response PAM-4 signal with seven levels. It is demonstrated, that a standard FFE is not enough for a transmission distance of > 0.6 km, while the use of an NLVE or FFE+MLSE is able to improve the transmission distance towards 1 km. The use of partial-response PAM-4 FFE (PR-FFE) in combination with a short memory MLSE is able to efficiently equalize the bandwidth limitations, showing more than 10-times BER improvement compared to standard NLVE or FFE+MLSE at a transmission distance of 1.6 km. Using a partial-response NLVE instead of an PR-FFE further performance improvement is achieved, resulting in BERs below the KP4 FEC-threshold with a BER-limit of 2E-4 after 1.6 km transmission distance, allowing error free operation.**

***Index Terms*—Adaptive equalizers, digital signal processing, nonlinear estimation, optical fiber communication, pulse amplitude modulation, vertical cavity surface emitting lasers.**

I. Introduction

The massive growth of cloud applications, services and infrastructure records an annual growth rate of 25 % for the overall global data center IP traffic [1]. Such enormous growth extensively drives the need for higher data rates together with a new generation of high-speed transceivers operating at 50 Gb/s and above. However, the environment of data centers, especially the short reach application, is very sensitive to cost, power consumption and footprint, requiring solutions with high capacities, low cost and small form factors [2].

Advanced modulation formats based on intensity modulation and direct detection (IM/DD) in combination with digital signal processing and coding will play an important role in future data center networks, as they enable to increase spectral efficiency and reduce lane count and thus cost and power dissipation [3], [4]. Recently, the IEEE P802.3bs Task Force has started to standardize four-level pulse-amplitude modulation (PAM-4) for the next generation of 400 GbE transmission over a single mode fiber (SMF). Three optical interface classes have been defined so far: 4x100 Gb/s parallel fiber transmission over 500 m (400GBASE-DR4), 8x50 Gb/s WDM transmission with 800 GHz carrier spacing over both, 2 km (400GBASE-FR8) and 10 km (400GBASE-LR8), all in the 1300 nm transmission window [5]. To further reduce the cost, the second generation will likely employ four wavelengths with 100 Gb/s each for the distances of 2 km and 10 km. Thus, the development of novel components and/or the use of advanced digital signal processing (DSP) is required to allow such transmission speed and reach.

TABLE I
TRANSMISSION RECORDS OF SINGLE-MODE VCSELS AT 1550 NM AND DIRECT DETECTION

Data rate	Format	DSP (Tx/ Rx)	Distance	FEC-limit	Ref.
56 Gb/s	NRZ	2-tap FFE/ none	2 km	None	[10]
56 Gb/s	PAM-4	none/ FFE and MLSE	2 km	3.8E-3 (OH* 7%)	[6]
56 Gb/s	PAM-4	4-tap FFE/ none	b2b	5.2E-4 (OH)	[14]
56 Gb/s	PAM-4	3-tap FFE/ 21-tap FFE	15 km	3.8E-3 (OH 7%)	[12]
84 Gb/s	PAM-4	3-tap FFE/ 21-tap FFE	1 km	3.8E-3 (OH 7%)	[12]
95 Gb/s	DMT	BL & PL/ 1-tap FFE	4 km	8E-3 (OH 20%)	[7]
115 Gb/s	DMT	BL & PL**/ 1-tap FFE	b2b	8E-3 (OH 20%)	[7]
56 Gb/s	DMT	BL & PL/ 1-tap FFE	12 km	3.8E-3 (OH 7%)	[11]
84 Gb/s	**PAM-4**	**3-tap FFE/ FFE, NLVE & MLSE**	**1.6 km**	**2E-4 (OH 3%)**	**This work**

* OH = required FEC overhead
** BL & PL = bit and power loading

The work was in part funded by the European Commission in the Marie Curie projects ABACUS, FENDOI and CEEOALAN and by the German ministry of education and research (BMBF) in project SpeeD under contract 13N1374.

Nicklas Eiselt is with the Department of Photonics Engineering, Technical University of Denmark and with ADVA Optical Networking SE in Meiningen, Germany (neiselt@advaoptical.com).

H. Griesser, A. Dochhan, M. Eiselt, and J.-P. Elbers are with ADVA Optical Networking SE in Meiningen and Martinsried, Germany.

J. Wei was with ADVA Optical Networking SE in Meiningen. He is now with Huawei Technologies Düsseldorf GmbH, European Research Center, Munich, Germany.

Robert Hohenleitner, Markus Ortsiefer and Christian Neumeyr are with Vertilas GmbH in Garching, Germany

J. J. Vegas Olmos and I. T. Monroy are with the Department of Photonics Engineering, Technical University of Denmark.

Recently increased research efforts - with steady improvement - have been made in developing long-wavelength high-speed vertical cavity surface emitting lasers (VCSELs) for next generation of data center applications [6]–[12]. Although VCSELs are mostly used for multi-mode applications, their low power consumption, the small footprint together with easy integration and the possibility of uncooled operation of up to 80° C make them also interesting for data center applications at long wavelengths [6], [13]. Furthermore, VCSELs are likely to be less expensive, compared to competing technologies such as distributed feedback laser (DFB) and Si Photonics [10]. In [10] error free operation of 56 Gb/s non-return to zero (NRZ) over 2 km SSMF was shown using a 1530 nm VCSEL and a two-tap feedforward pre-emphasize driver. For applying higher order modulation formats forward error correction (FEC) encoding is needed. Fotini et al. showed 56 Gb/s PAM-4 over up to 2 km SSMF with an 18-GHz bandwidth VCSEL at 1530 nm [6]. A 7-% hard-decision (HD) FEC was assumed and powerful equalization at the receiver side was needed. In [14] also 56 Gb/s PAM-4 with bit error rates (BERs) below 1E-6 was demonstrated for optical back-to-back (b2b) enabled by a 4-tap pre-emphasize driver and a 22-GHz VCSEL at 1533 nm. And in [12] we demonstrated 56 Gb/s and 84 Gb/s PAM-4 transmission over up to 15 km and 1 km SSMF, respectively, with a 18-GHz long-wavelength VCSEL at 1525 nm using simple transceiver DSPs and the assumption of HD-FEC with a BER-limit of 3.8E-3. Multicarrier formats in combination with long-wavelength VCSELs have also been investigated. Xie et al. [7] demonstrated up to 115 Gb/s (~ 95.8 Gb/s net rate) discrete multi-tone (DMT) transmission with a single 1550 nm VCSEL assuming 20 % HD-FEC overhead with a BER-limit of 1.5E-2. In [11] 56-Gb/s single side-band DMT transmission was demonstrated over up to 12 km SSMF, using an 18-GHz VCSEL at a transmission wavelength of 1530 nm. Again a 7 % FEC with a BER-limit of 3.8E-3 was assumed.

However, in addition to the mentioned advantages of VCSELs, these publications also reveal some serious obstacles when using VCSELs at 1550 nm. Chromatic dispersion in combination with the frequency chirp of the VCSEL and the low extinction ratio (normally around 3 to 5 dB) result in a tight power budget and a short transmission distance [15], which becomes even worse at higher data rates. In addition, VCSEL nonlinearities and a maximum bandwidth of around 22 GHz [14] impose further challenges to the system. Powerful signal processing/equalization is thus required to allow the transmission of data rates of > 100 Gb/s using VCSELs and to enable cost-efficient high capacity links. In this paper, we extend the results shown in [12] by applying nonlinear equalization based on the Volterra-theorem and maximum likelihood sequence estimation (MLSE). With such equalization techniques, transmission results of 84 Gb/s PAM-4 below the standard KP4 FEC-threshold with a BER-limit of 2E-4 are demonstrated over up to 1.6 km SSMF using a 20-GHz VCSEL at a transmission wavelength of 1525 nm. The VCSEL is based on Vertilas' unique InP Buried Tunnel Junction (BTJ) design and features a very short optical cavity.

This paper is organized as follows. In section II the design and the characteristics of the VCSEL are presented and discussed. In section III, the experimental setup together with the applied DSP at the transmitter as well as at the receiver are outlined in detail. Section IV reports and discusses the experimental results obtained with the different equalizer approaches. Finally, conclusions are drawn in section V.

II. VCSEL Structure

The deployed single mode short cavity VCSEL is based on Vertilas' unique InP Buried Tunnel Junction (BTJ) design and features a very short optical cavity. A detailed cross section of the VCSEL design can be found in [10].

The short cavity concept has been realized by deploying dielectric material for both the top and bottom mirror of the VCSEL. The high refractive index of the dielectric material allows to realize a very high reflectivity distributed bragg reflector (DBR) with only 3.5 mirror pairs, which is much thinner compared to a semiconductor DBR with the required 30-40 mirror pairs. This reduces the effective cavity length by more than 50 % and greatly reduces the photon lifetime, an effect that directly increases the bandwidth of the device.

The InP BTJ VCSEL concept includes a specific processing step, where most of the semiconductor material is being etched away, producing a defined semiconductor mesa structure for each laser on the wafer. The void resulting from this manufacturing step is subsequently filled with benzocyclobutene (BCB), a polymer material that is spun onto the wafer and cured

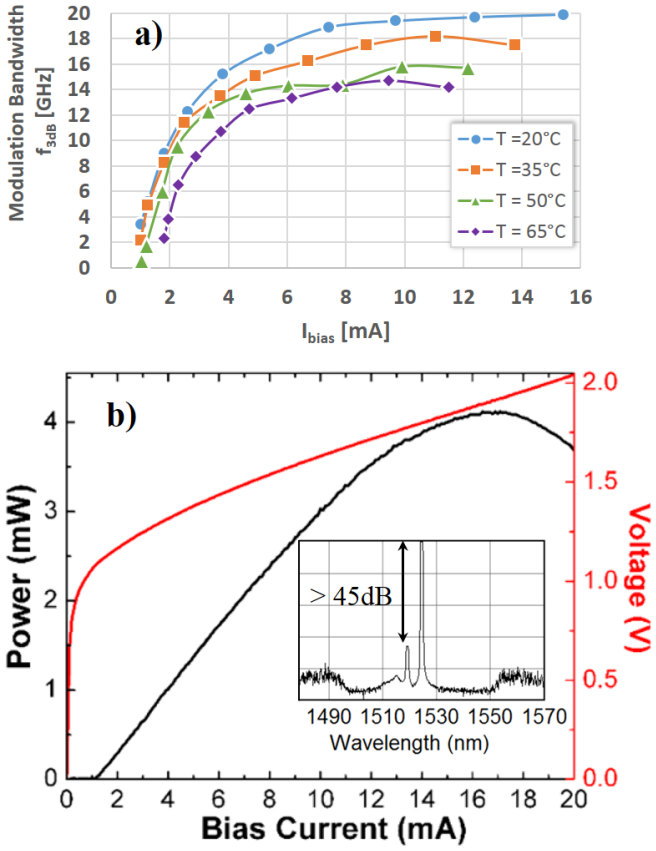

Fig. 1: (a) Modulation bandwidth vs. bias current of short cavity VCSEL at different temperatures, (b) LIV and UI characteristics and (c) unmodulated transmission spectrum of the VCSEL.

under high temperatures. The mesa diameter of the design under test (DUT) has been further optimized to keep the parasitics to a minimum. Both, the reduced photon lifetime and the decreased parasitics could greatly improve the modulation bandwidth to a maximum of 20 GHz at room temperature, as indicated in Fig. 1(a). At higher temperature e.g. 65 °C the maximum bandwidth is reduced to approximately 15 GHz. This maximum modulation bandwidth can be achieved at a very low operating current of 11 mA. Particular attention for this laser design has also been given to achieve a very low threshold current (I_{th}) of less than 1 mA and a high optical power of 4 mW, as shown in Fig. 1(b). The laser design includes wave guiding effects, enabling to suppress side modes and favor the main mode to realize a high side mode suppression ratio of more than 45 dB.

In summary, the device used for these experiments is a single mode and polarization stable 1550 nm VCSEL with excellent device parameters, such as a very low threshold current, high side mode suppression ratio (SSMF), high bandwidth and very low power consumption. The InP technology allows to produce lasers for the various communications applications in the O-Band, C-Band and L-band range.

III. Transmission Setup and DSP

A. Experimental Setup

The experimental setup for the PAM-4 transmission including the offline DSP units at the transmitter and the receiver side is shown in Fig. 2. Furthermore, the optical PAM-4 eye diagram at a data rate of 84 Gb/s (symbol rate 42 GBd) obtained at the VCSEL output and the VCSEL die with perpendicularly placed fiber and the electrical probes are depicted as insets of Fig. 2.

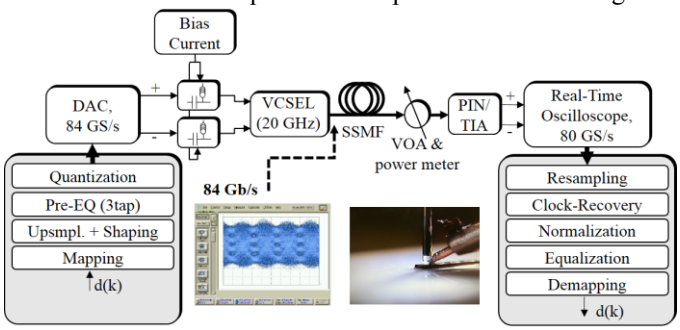

Fig. 2: Experimental setup and offline DSP steps.

For transmission, following components are used: The offline generated PAM-4 signal is converted into an electrical signal via a Socionext digital-to-analog converter (DAC), which operates at a sampling speed of 84 GS/s. The nominal resolution of this DAC is 8 bit, and the 3-dB bandwidth is around 15 GHz [16], [17]. Afterwards, the differential outputs of the DAC are passed through two bias-tees and two electrical probes directly to the VCSEL die. No driver was used and the differential output swing of the DAC was around 800 mV peak-to-peak. For transmission, a bias current of 12 mA was chosen, which gives the best trade-off between extinction, bandwidth of the VCSEL and optical output power (see section II). At this bias point, the maximum output power into the fiber was around +1 dBm, and the transmission wavelength was approximately 1525 nm. To couple the light into the fiber, a lensed fiber was placed perpendicularly over the VCSEL die. The optical link setup consisted of a conventional SSMF, a variable optical attenuator (VOA) with an integrated power monitor, and a PIN-photodetector (Picometrix PT-28E) integrated with a linear trans-impedance amplifier (PIN/TIA) with a combined bandwidth of 30 GHz. Subsequently, an 80-GS/s real-time oscilloscope from Agilent with 29 GHz bandwidth digitized the received signal and stored it for further offline post processing.

B. DSP at transmitter and receiver

At the transmitter side, a gray-coded PAM-4 signal is generated from two binary De Bruijn-sequences of length 2^{15}, with one of the two sequences shifted by half the sequence length to ensure sufficient decorrelation. In the next step, the signal is up-sampled by a factor of two and shaped with a rectangular filter in the time-domain, before a 3-tap pre-equalizer is applied. The pre- and post-cursor are adjusted for best BER in optical back-to-back (b2b) mode. Finally, the signal is quantized and sent to the 84-GS/s DAC to generate the electrical PAM-4 signal.

In this paper different equalizers at the receiver shall be evaluated and compared. To this aim, the signal is first resampled to four-fold oversampling, the DC-component is removed and a clock recovery is applied by estimating the phase of the spectral line at symbol rate [18]. Afterwards the signal is downsampled by a factor of two, normalized and equalized. Finally, an optimum threshold detector is used and the BER is counted.

Three different equalizers are implemented and combined with each other. A simple FFE based on the LMS-criterion with a step-size of $\mu = 0.001$ is applied for all transmission scenarios. The FFE is then extended towards a nonlinear FFE, which can address the nonlinear behaviour of the VCSEL and of the photodiode and is referred to as nonlinear Volterra equalizer (NLVE) [19]. Utilizing the Volterra kernels, the output of this equalizer can be written as

$$\begin{aligned}\hat{d}(k) = &\sum_{n_1=0}^{N_1} h_{n_1} x(Wk - n_1) \\ &+ \sum_{n_1=0}^{N_1}\sum_{n_2=n_1}^{N_2} h_{n_1,n_2} \prod_{i=1}^{2} x(Wk - n_i) \\ &+ \sum_{n_1=0}^{N_1}\sum_{n_2=n_1}^{N_2}\sum_{n_3=n_2}^{N_3} h_{h_{n_1,n_2,n_3}} \prod_{i=1}^{3} x(Wk - n_i)\end{aligned} \quad (1)$$

with $h_{n_1}, h_{n_1,n_2}, h_{n_1,n_2,n_3}$ representing the first, second and third order Volterra kernels and N_1, N_2, N_3 the kernel depth. W is the oversampling factor and $x(k)$ is the received signal at the sampling point k. Again, the LMS-criterion with a step-size of μ=0.001 is used to determine the kernel values.

The third equalizer to be considered here is the MLSE based on the Euclidian distance metric and the Viterbi algorithm [20], [21]. To reduce the complexity of the MLSE, we only use it in combination with a preceding FFE or a NLVE. In this case, the FFE (NLVE) is basically used to shorten the impulse response, requiring less memory for the MLSE. A more detailed analysis of these equalizers will be done in the following sections.

IV. Results and Discussions

In this section the results achieved with the different equalizer structures are shown and discussed. The whole equalizer structure based on the LMS-criterion is shown in a generic block diagram in Fig. 3.

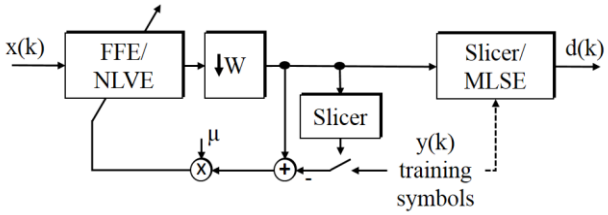

Fig. 3: Block diagram of the adaptive equalization structure. W is the downsampling factor, μ the step-size, x(k) the received signal, y(k) the training symbols and d(k) the decoded symbols.

A. Linear FFE

At first, the performance of a simple FFE is investigated and evaluated. In Fig. 4 the BER vs. received optical input power (ROP) into the PIN/TIA for different transmission distances is depicted. Several eye diagrams obtained after equalization are added as insets to show the signal quality after the FFE. A fractionally-spaced FFE with optimum tap coefficient count of 21 is applied, beyond which no further improvement is achieved as identified in Fig. 7(a). Even at the distance of 1.63 km 21 equalizer coefficients are sufficient. Assuming the currently standardized KP4 (RS(544,514,10)) FEC-threshold with a pre-FEC BER-limit of 2E-4 [5], (visualized as a solid black line in the plots) only for the optical back-to-back (b2b) case BERs below the threshold are obtained. At distances of 0.63 km or longer a significant performance degradation is observed, indicating that a simple FFE is not enough for such an application. This can also be verified by the equalized eye diagram, which is still completely closed for 1.63 km.

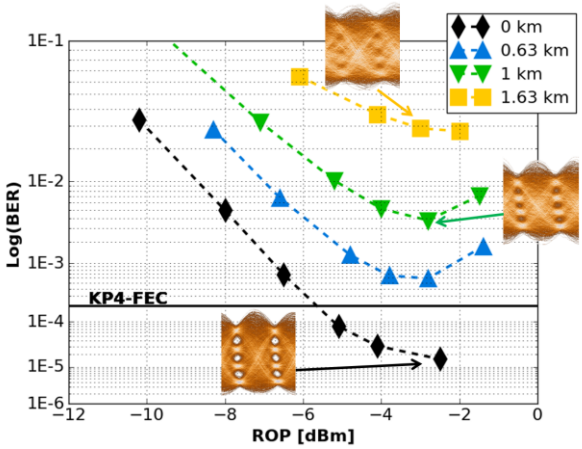

Fig. 4: Receiver sensitivity of 84 Gb/s PAM-4 at different transmission distances using simple FFE with 21 filter coefficients. In the inset, equalized eye diagrams are shown.

For all the evaluated equalizer combinations, training symbols are used at startup. In principle, the equalizer could also work in a completely blind mode [17], however, we experienced a more stable performance of the equalizer with training symbols, especially in case of strong distortions. The first 5000 samples of the received signal are used as training symbols and afterwards the equalizer is switched to a blind adaptive mode with a hard decision in the equalizer. As the training is part of the initial equalizer convergence process, we do not assume additional overhead for the equalizer training. This assumes a bi-directional connection with a special start-up protocol. For the measurements, the symbols used in this convergence process are not counted for the BER-calculation. In Fig. 5 the adaption speed of the FFE is shown by means of the sampling points of the equalized signal and the absolute value of the LMS-error. The equalizer converged to a stable working point already after 5000 symbols.

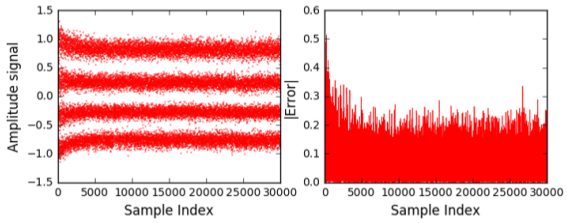

Fig. 5: Adaption speed of the FFE with 21 filter coefficients depicted by means of the time signal (left) and the LMS-error (right).

As mentioned in the previous section, a fixed step-size of μ = 0.001 was used for all measurement results, which, as shown in Fig. 6, is close the optimum. A bigger step-size, e.g. μ = 0.01, offers a fast convergence together with a fast tracking. However, it also results in a bigger residual error and thus, a worse BER performance. On the other hand, a smaller step-size may result in a smaller residual error, however, it also needs a longer convergence time and has a slower tracking capability. Using a fixed convergence length of only one sequence (2^{15} symbols), there is an optimum step-size that provides best performance. If we assume a longer convergence time, the performance can be further improved, as indicated by the round markers in Fig. 6.

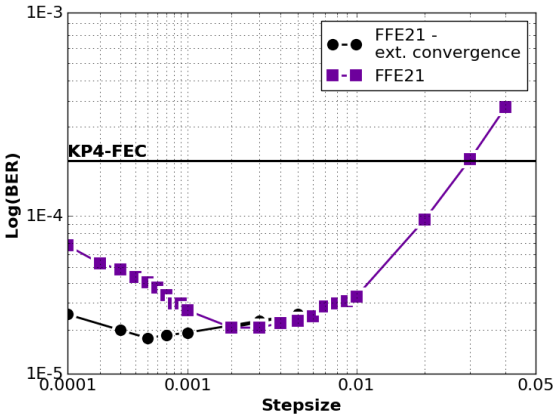

Fig. 6: Optimization of step-size of the LMS algorithm in case of an FFE with 21 filter coefficients and for a transmission distance of 0 km.

It is often desired to use the equalizer in a symbol-spaced mode, as less filter-coefficients are needed compared to a fractionally-spaced equalizer. However, a good clock recovery is required in this case, as symbol-spaced equalization is very sensitive to phase shifts. In Fig. 7(b) the performance of a fractionally-spaced FFE and a symbol-spaced FFE are illustrated for the optical b2b case. A very similar performance is seen with symbol-spaced FFE being slightly worse. The performance difference becomes more significant at very low BER-values. Nevertheless, the results indicate that clock-recovery is working reasonably; allowing in principle also the use of symbol-

spaced equalization for such an application. This is also justified by the results in Fig. 8, where the power density spectra (PDS) of the received signal after the ADC and of the absolute squared signal used within the clock-recovery algorithm for b2b and for 1.6 km are shown. Although chromatic dispersion heavily limits the bandwidth at 1.6 km, the spectral lines at the baud rate can still be clearly distinguished.

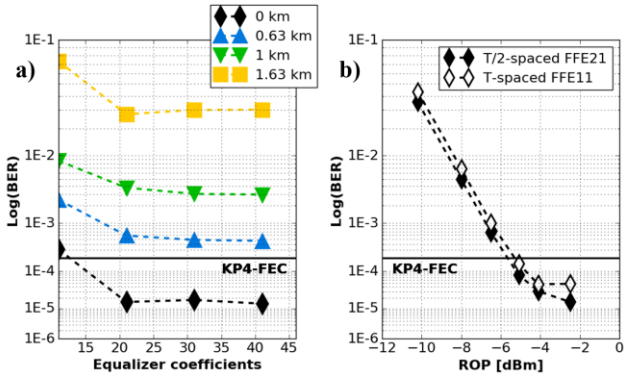

Fig. 7: a) Optimization of the FFE equalizer coefficients for 84 Gb/s PAM-4 transmission and b) comparison between a fractionally-spaced (T/2-spaced) and symbol-spaced (T-spaced) FFE for optical back-to-back.

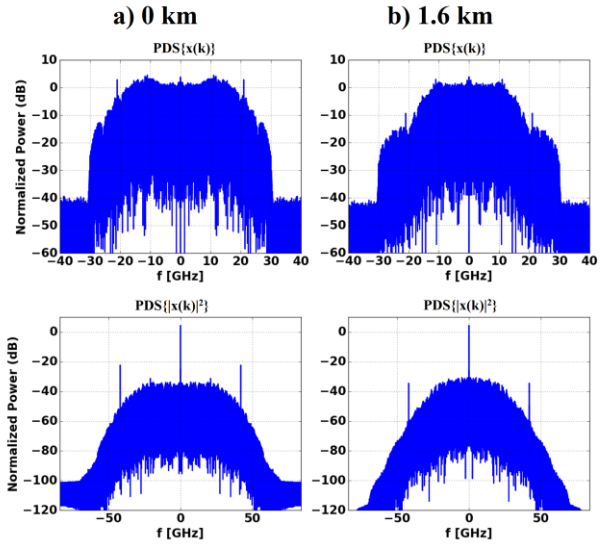

Fig. 8: Power density spectra of the received signal and after $|.|^2$ operation for clock-recovery for the cases a) 0 km and b) 1.6 km.

B. NLVE

Since Fig. 4 shows that a simple FFE is not enough to transmit over distances of 0.63 km or more by considering the KP4 FEC-threshold, stronger equalization is required to improve the performance at longer distances. Transmitting PAM-4 at 84 Gb/s and at a transmission wavelength of 1525 nm, chromatic dispersion becomes a severe limitation, impacting the performance strongly. This is identified by comparing the eye-diagrams at optical b2b and 0.63-km SSMF transmission, where the latter one is very much destroyed (Fig. 4 and Fig. 9). In addition, the PIN/TIA gets nonlinear at higher input power values, as indicated by the achieved results in Fig. 4. At input power values of more than – 2 dBm the performance is degraded. And finally, the VCSEL shows a power level dependent delay, which accumulates in an asymmetrical PAM-4 eye diagram (skewing in the received eye diagram), similar to what has been described for DMLs [22], [23]. A normal FFE considers only linear distortions and is therefore unable to compensate for the power dependent asymmetry. In principle, the NLVE should be able to compensate for this asymmetry, if enough kernels are considered. This can be verified in Fig. 9, where the received and equalized eye diagrams at a transmission distance of 0.63 km and an input power of – 4 dBm are shown. For the FFE, 21 coefficients are used, while the NLVE consists of 21 linear coefficients and a second-order kernel depth of $N_2 = 9$, denoted as FFE 21-9 in this paper. Using a kernel depth of $N_2 = 9$, 45 additional equalizer coefficients are needed. The FFE is able to open the eye, but, as expected, an eye skew is still present. The eye diagram after the NLVE shows no skew anymore and enables better eye opening. Moreover, the lower eye is much less distorted after the NLVE, resulting in very similar eye openings for all three eyes. The nonlinear behaviour of the used PIN/TIA results in a smaller eye opening of the lower eye.

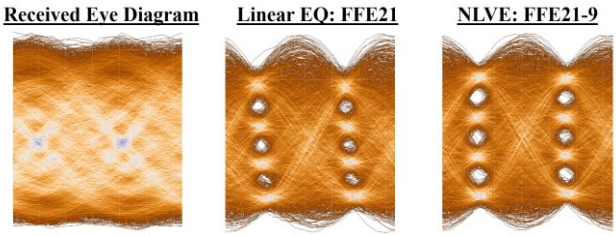

Fig. 9: Received and equalized eye diagrams at a transmission distance of 0.63 km.

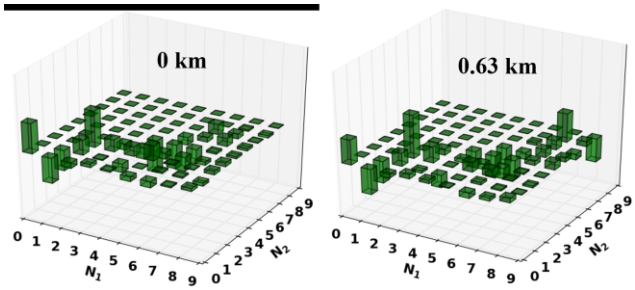

Fig. 10: Second order kernels with a kernel depth of $N_2 = 9$ at a transmission distance of 0 km and 0.63 km and at a ROP of – 4 dBm.

In Fig. 10 the Kernel values of second order with a kernel depth of $N_2 = 9$ are depicted for the b2b-case and for 0.63 km SSMF transmission. Only the kernels along the diagonal have higher values, while the other kernels are nearly zero. In principle, these could be excluded in order to reduce complexity as they do not have any impact on the performance.

Finally, the performance of the NLVE for the different transmission distances is shown in Fig. 11(a). In addition, the BER values achieved with an FFE of 21 coefficients are added as a dotted line and filled diamond markers for comparison. A significant performance improvement is obtained at higher input power values by using the NLVE. At lower input power, the NLVE does not improve the system further, as noise is the dominant impairment. A second order kernel depth of $N_2 = 9$ is required to reach BERs below the KP4 FEC-threshold in case of 1 km SSMF distance. At shorter distances, even $N_2 = 3$ improves the performance significantly compared to a simple FFE, achieving BER values below the FEC-threshold for 0.63 km transmission. A third order kernel with $N_3 = 3$, result-

ing in the combination FFE21-9-3, further improves the performance slightly. As complexity of the NLVE increases dramatically with Kernel depth and Kernel number, no further evaluation is done. Moreover, also the NLVE is not able to efficiently equalize the distortions at a transmission distance of 1.63 km, requiring a different equalizer solution.

C. *MLSE*

The MLSE is known to be the optimum receiver for linear bandwidth-limited channels [21], [24]. As complexity of such an equalizer grows exponentially with memory, the use of an FFE in front of the MLSE represents an effective solution to shorten the impulse response of the system and reduce the required memory of the MLSE. Basically, the MLSE replaces the hard decision threshold after the FFE as shown in Fig. 3. Hence, a fractionally-spaced FFE of 21 coefficients in combination with an MLSE of different memory sizes is chosen. The MLSE runs at 1 sample per symbol and operates statically; meaning it is trained at the beginning and not changed afterwards any more. Along the lines of [25] we estimate the mean of the probability density functions (PDFs) of a channel matrix using 2^{15} received samples and the corresponding digital data from the first period of the sent sequence. This assumes an additive Gaussian noise distribution with equal variance for all PDFs. Subsequently, the branch metrics for the Viterbi trellis is calculated as being proportional to the squared Euclidian distance of the received sample and the corresponding mean value.

In Fig. 11(b) the results of the FFE-MLSE and NLVE-MLSE combinations are shown. The memory size is indicated by the numeral, e.g. MLSE1 indicates a memory m of one, which corresponds to 4^{m+1}=16 states for the Viterbi algorithm. A memory of two corresponds to a 64 states and a memory of three to 256 states. Although the FFE tries to shorten the impulse response to a length of one, a significant performance improvement is observed by using more memory at higher input power values. Basically, the more memory the MLSE uses, the better the performance against nonlinearities. A memory of three (MLSE3) is required to reach the KP4 FEC-threshold for 1 km transmission, while a memory of two is enough for the transmission distance of 0.63 km. However, a significant performance improvement can be observed when using a memory of three compared to a memory of two at input powers of – 2 dBm. An MLSE1 does not add any significant improvement to the performance of a simple FFE and a hard decision. Some small performance improvements are obtained by replacing the FFE-MLSE with an NLVE-MLSE combination. However, less memory of the MLSE is required, as now also the NLVE equalizes part of the nonlinear distortions. Thus, a low-complex NLVE in combination with an MLSE2 is able to achieve nearly the same performance as an FFE-MLSE3 combination. At a transmission distance of 1.63 km, however, no combination is able to reach to the KP4 FEC-threshold.

In recent papers the use of 100 Gb/s partial response PAM-4 (PR-PAM-4) has been proposed for short reach applications [17], [26], [27], representing an effective solution to transmit 100 Gb/s over bandwidth limited channels. The influence of

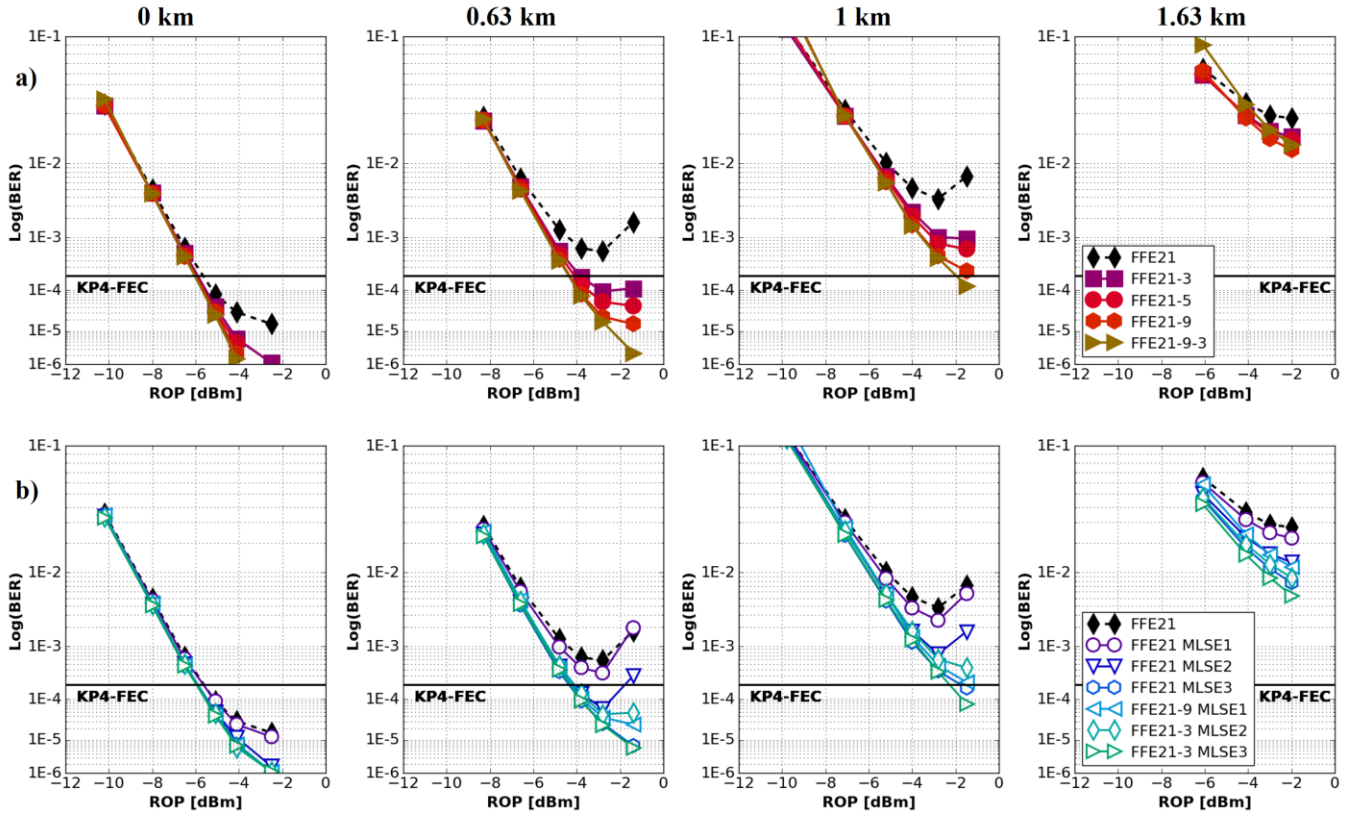

Fig. 11: Receiver sensitivity at different transmission distances at 84 Gb/s PAM-4 with a) using NLVE with different number of kernels and b) using a combination of FFE-MLSE or NLVE-MLSE.

chromatic dispersion can be seen as a form of bandwidth limitation. Indeed, the received eye diagrams after 0.63 km or 1 km (Fig. 9 and Fig. 12) indicate seven levels instead of four, very similar to a partial-response PAM-4 signal. Hence, the FFE is switched to a partial-response decoder (PR-FFE) by equalizing on the seven levels. The partial response filtering is done in the receiver as part of the PR-FFE. To achieve this behavior of the PR-FFE, the first 5000 samples, which served as a training sequence were partial response encoded by means of equation (2) before using them as target value for the error calculation of the filter adaption:

$$y(k) = y(k) + y(k-1). \qquad (2)$$

In blind mode a hard decision based on six hard decision thresholds is used in the equalizer. An MLSE is applied afterwards to equalize the residual inter-symbol interference and decode the PAM-4 signal. The eye diagrams after partial response equalization are illustrated in Fig. 12, using a PR-FFE with 21 coefficients and also a PR-NLVE with 21 linear coefficients and a second order kernel depth of $N_2 = 9$. Seven levels after equalization can be clearly distinguished.

The obtained time domain equalizer taps together with the corresponding PDS of the FFE and the PR-FFE are displayed in Fig. 13a) and 13b) for a transmission distance of 1 km. It is shown, that the FFE has to strongly amplify the higher frequencies in order to equalize the strong bandwidth limitations of the system, resulting in significant noise enhancement and thus performance degradation. In contrast, the PR-FFE operates more like a band limiting filter, reducing the influence of noise.

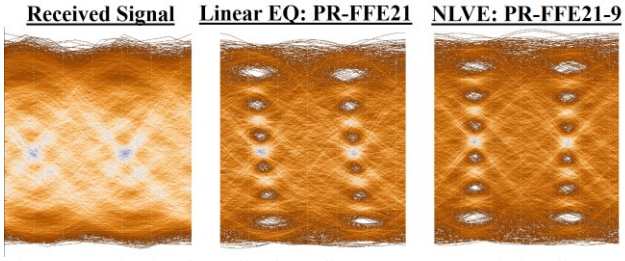

Fig. 12: Received and equalized eye diagrams at a transmission distance of 1 km using a partial response equalizer.

Finally, Fig. 14 depicts the results for the transmission distances of 1 km and 1.63 km SSMF using a linear PR-FFE (Fig. 14(a)) or a nonlinear PR-NLVE (Fig. 14(b)) together with an MLSE. The distances of 1 km and 1.63 km are considered here, as only at these distances a performance improvement with partial-response equalization was observed. In case of 1.63 km and linear PR-FFE, BERs around the KP4 FEC-threshold are obtained, resulting in a significantly better performance compared to the FFE-MLSE combination (Fig. 11). Moreover, an MLSE2 is sufficient, as no further improvement is achieved with an MLSE3. However, the figure also shows, that BERs below the KP4 FEC-threshold for the 1.6 km case are only achieved with the very complex combination FFE21-15 MLSE2, which requires 141 NLVE coefficients and 64 MLSE states. In table II, the most significant results achieved with the different equalizer combinations are summarized.

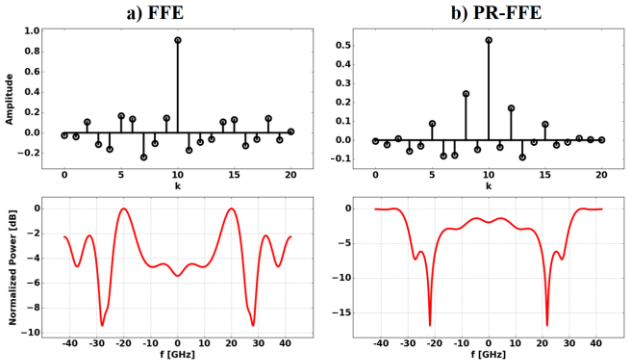

Fig. 13: Time domain equalizer taps and their spectral behaviour obtained for a transmission distance of 1 km of a) the normal FFE and b) the PR-FFE. Both equalizers operate as a T/2-spaced equalizer.

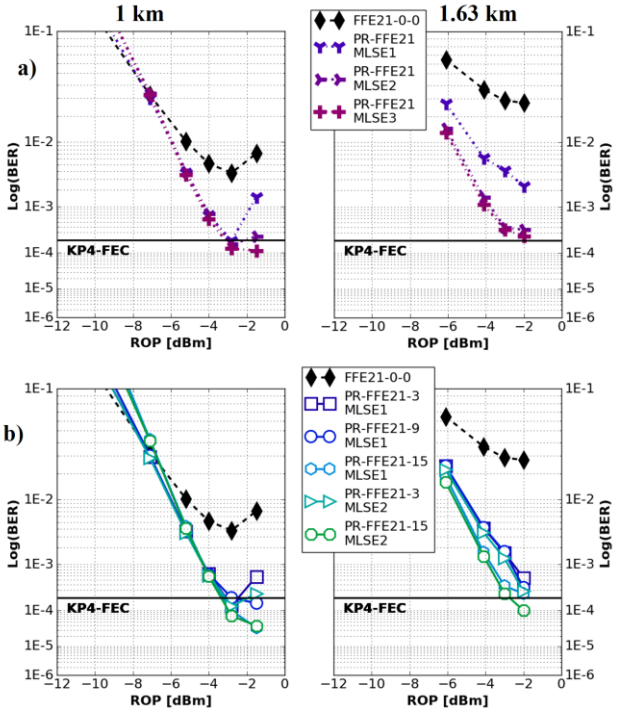

Fig. 14: Receiver sensitivity of 84 Gb/s PAM-4 at 1 km and 1.63 km using a) a linear partial response FFE and an MLSE and b) a partial-response NLVE with an MLSE.

TABLE II
SUMMARY OF ACHIEVED TRANSMISSION RESULTS WITH THE DIFFERENT EQUALIZER COMBINATIONS

Equalizer	Max. Distance	BER
FFE 21	b2b	2E-5
FFE21-9-3	1 km	1E-4
FFE21 MLSE3	1 km	2E-4
FFE21-9 MLSE3	1 km	8E-5
PR-FFE21 MLSE1	1 km	1E-4
PR-FFE21-15 MLSE2	1.6 km	9E-5

V. CONCLUSION

On the road to 100 Gb/s transmission with long-wavelength VCSELs and direct detection, we demonstrated 84 Gb/s PAM-4 over 1.6 km SSMF at a transmission wavelength of 1525 nm using a 20-GHz VCSEL based on a BTJ design. It is shown, that due to chromatic dispersion and VCSEL nonlinearities, a

linear equalizer at the receiver is not sufficient to achieve performances below the KP4 FEC-threshold. Different combinations of FFE, NLVE and MLSE have been experimentally investigated, evaluated and compared. A significant performance improvement is achieved by using the NLVE, working either as a normal PAM-4 equalizer or as a partial-response equalizer combined with a low memory MLSE. This approach achieves BERs below the KP4 FEC-threshold with a BER-limit of 2E-4 even after 1.63 km of transmission distance.

REFERENCES

[1] Cisco, "Cisco Global Cloud Index : Forecast and Methodology , 2014–2019," *White Pap.*, pp. 1–41, 2014.

[2] M. A. Mestre, H. Mardoyan, C. Caillaud, R. Rios-Müller, J. Renaudier, P. Jennevé, F. Blache, F. Pommereau, J. Decobert, F. Jorge, P. Charbonnier, A. Konczykowska, J. Y. Dupuy, K. Mekhazni, J. F. Paret, M. Faugeron, F. Mallecot, M. Achouche, and S. Bigo, "Compact InP-Based DFB-EAM Enabling PAM-4 112 Gb/s Transmission over 2 km," *J. Light. Technol.*, vol. 34, no. 7, pp. 1572–1578, 2016.

[3] J. Wei, Q. Cheng, R. V. Penty, I. H. White, and D. G. Cunningham, "400 Gigabit Ethernet using advanced modulation formats: Performance, complexity, and power dissipation," *IEEE Commun. Mag.*, vol. 53, no. 2, pp. 182–189, 2015.

[4] I. Lyubomirsky and W. A. Ling, "Advanced Modulation for Datacenter Interconnect," in *Optical Fiber Communication Conference*, 2016, p. W4J.3.

[5] "IEEE P802.3bs™/D1.2 Draft Standard for Ethernet Amendment: Media Access Control Parameters, Physical Layers and Management Parameters for 400 Gb/s Operation," 2016. [Online]. Available: http://www.ieee802.org/3/bs/.

[6] F. Karinou, C. Prodaniuc, N. Stojanovic, M. Ortsiefer, A. Daly, R. Hohenleitner, B. Kogel, and C. Neumeyr, "Directly PAM-4 Modulated 1530-nm VCSEL Enabling 56 Gb/s/ lamda Data-Center Interconnects," *IEEE Photonics Technol. Lett.*, vol. 27, no. 17, pp. 1872–1875, 2015.

[7] C. Xie, P. Dong, S. Randel, D. Pilori, P. Winzer, S. Spiga, B. Kögel, C. Neumeyr, and M.-C. Amann, "Single-VCSEL 100-Gb/s Short-Reach System Using Discrete Multi-Tone Modulation and Direct Detection," in *Optical Fiber Communication Conference*, 2015, no. Tu2H.2.

[8] M. Ortsiefer, J. Rosskopf, B. Kögel, A. Daly, M. Görblich, Y. Xu, C. Gréus, and C. Neumeyr, "Long Wavelength VCSELs with Enhanced Temperature and Modulation Characteristics," in *IEEE International Semiconductor Laser Conference*, 2014.

[9] M. Müller, W. Hofmann, T. Gründl, M. Horn, P. Wolf, R. D. Nagel, E. Rönneberg, G. Böhm, D. Bimberg, and M. C. Amann, "1550-nm high-speed short-cavity VCSELs," *IEEE J. Sel. Top. Quantum Electron.*, vol. 17, no. 5, pp. 1158–1166, 2011.

[10] D. M. Kuchta, T. N. Huynh, F. E. Doany, L. Schares, C. W. Baks, C. Neumeyr, A. Daly, B. Kogel, J. Rosskopf, and M. Ortsiefer, "Error-free 56 Gb/s NRZ modulation of a 1530-nm VCSEL link," *J. Light. Technol.*, vol. 34, no. 14, pp. 3275–3282, 2016.

[11] A. Dochhan, N. Eiselt, R. Hohenleitner, H. Griesser, and M. Eiselt, "56 Gb/s DMT Transmission with VCSELs in 1.5 um Wavelength Range over up to 12 km for DWDM Intra-Data Center Connects," in *European Conference on Optical Communication, ECOC*, 2016, no. Tu.3.C.4.

[12] N. Eiselt, H. Griesser, J. Wei, A. Dochhan, and R. Hohenleitner, "Experimental Demonstration of 56 Gbit/s PAM-4 over 15 km and 84 Gbit/s PAM-4 over 1 km SSMF at 1525 nm using a 25G VCSEL," in *European Conference on Optical Communication, ECOC*, 2016, no. Th.1.C.1.

[13] A. Larsson, J. S. Gustavsson, P. Westbergh, E. Haglund, E. P. Haglund, and E. Simpanen, "High-Speed VCSELs for Datacom," in *European Conference on Optical Communication, ECOC*, 2016, p. Th.1.C.3.

[14] W. Soenen, R. Vaernewyck, X. Yin, S. Spiga, and M. Amann, "56 Gb/s PAM-4 Driver IC for Long-Wavelength VCSEL Transmitters," in *European Conference on Optical Communication, ECOC*, 2016, p. Th.1.C.4.

[15] J. Zhou, S. Member, C. Yu, S. Member, H. Kim, and S. Member, "Transmission Performance of OOK and 4-PAM Signals Using Directly Modulated 1.5-μm VCSEL for Optical Access Network," *J. Light. Technol.*, vol. 33, no. 15, pp. 3243–3249, 2015.

[16] S. Van Der Heide, N. Eiselt, H. Griesser, J. José, and V. Olmos, "Experimental Investigation of Impulse Response Shortening for Low-Complexity MLSE of a 112-Gbit/s PAM-4 Transceiver," *Eur. Conf. Opt. Commun. ECOC*, no. 1, pp. 115–117, 2016.

[17] N. Stojanovic, Z. Qiang, C. Prodaniuc, and F. Karinou, "Performance and DSP complexity evaluation of a 112-Gbit/s PAM-4 transceiver employing a 25-GHz TOSA and ROSA," in *2015 European Conference on Optical Communication (ECOC)*, 2015, p. Tu.3.4.5.

[18] M. Oerder and H. Meyr, "Digital Filter and Square Timing Recovery," *IEEE Trans. Commun.*, vol. 36, no. 5, pp. 605–612, 1988.

[19] C. Xia and W. Rosenkranz, "Nonlinear electrical equalization for different modulation formats with optical filtering," *J. Light. Technol.*, vol. 25, no. 4, pp. 996–1001, 2007.

[20] G. D. Forney, "Maximum-Likelihood Sequence Estimation of Digital Sequences in the Presence of Intersymbol Interference," *IEEE Trans. Inf. Theory*, vol. 18, no. 3, pp. 363–378, 1972.

[21] G. Ungerboeck, "Adaptive Maximum-Likelihood Receiver for Carrier-Modulated Data-Transmission Systems," *IEEE Trans. Commun.*, vol. 22, no. 5, pp. 624–636, 1974.

[22] A. S. Karar, J. C. Cartledge, J. Harley, and K. Roberts, "Electronic pre-compensation for a 10.7-Gb/s system employing a directly modulated laser," *J. Light. Technol.*, vol. 29, no. 13, pp. 2069–2076, 2011.

[23] N. Kikuchi, R. Hirai, and T. Fukui, "Non-linearity Compensation of High-Speed PAM4 Signals from Directly-Modulated Laser at High Extinction Ratio," in *European Conference on Optical Communication, ECOC*, 2016.

[24] O. E. Agazzi, M. R. Hueda, H. S. Carrer, and D. E. Crivelli, "Maximum-likelihood sequence estimation in dispersive optical channels," *J. Light. Technol.*, vol. 23, no. 2, pp. 749–763, 2005.

[25] G. Bosco, P. Poggiolini, and M. Visintin, "Performance analysis of MLSE receivers based on the square-root metric," *J. Light. Technol.*, vol. 26, no. 14, pp. 2098–2109, 2008.

[26] L. F. Suhr, J. J. V. Olmos, B. Mao, X. Xu, G. N. Liu, and I. T. Monroy, "112-Gbit/s x 4-Lane Duobinary-4-PAM for 400GBase," in *European Conference on Optical Communication, ECOC*, 2014, p. Tu.4.3.2.

[27] X. Xu, E. Zhou, G. N. Liu, T. Zuo, Q. Zhong, L. Zhang, Y. Bao, X. Zhang, J. Li, and Z. Li, "Advanced modulation formats for 400-Gbps short-reach optical inter-connection," *Opt. Express*, vol. 23, no. 1, p. 492, 2015.